Dynamic ON-State Resistance Test and Evaluation of GaN Power Devices Under Hard- and Soft-Switching Conditions by Double and Multiple Pulses

Rui Li, *Student Member, IEEE*, Xinke Wu, *Member, IEEE*, Shu Yang, *Member, IEEE*, and Kuang Sheng, *Senior Member, IEEE*

***Abstract*—The dynamic ON-state resistance (R_{DSON}) behavior of commercial GaN devices is very important for a GaN-based converter. Since the zero-voltage switching techniques are popular in high-frequency power conversion, a dynamic R_{DSON} test board integrating both hard- and soft-switching test circuits is built in this study. Two types of commercial GaN devices are tested and compared under hard- and soft-switching conditions by double-pulse and multipulse test modes, respectively. It has been found that their dynamic R_{DSON} exhibit different behaviors depending on the OFF-state voltage and frequency under hard- and soft-switching conditions due to different device technologies, which should be taken fully into account for GaN-based converter design and loss estimation. In order to simulate the R_{DSON} behavior in a steady-state operating converter, a multipulse measurement has been implemented, the results of which are compared with that of double-pulse test. Furthermore, the primary trapping mechanisms responsible for dynamic R_{DSON} increase under different switching conditions are identified and verified by the numerical device simulation using Silvaco TCAD tool.**

***Index Terms*—Current collapse, dynamic ON-state resistance, GaN devices, hard switching, soft switching.**

I. Introduction

GaN power devices exhibit great performance in high-frequency applications. However, these devices often suffer from current collapse, leading to an increase of R_{DSON} after switching from high-voltage OFF state. The increase of dynamic R_{DSON} originates primarily from electron trapping by surface traps in the gate-to-drain access region and buffer traps beneath the two-dimensional electron gas (2DEG) channel induced by gate injection in the OFF state [1] or hot electrons injection from channel during the switching transients [2]. Due to the variation of R_{DSON} with different voltage and frequency conditions, it

Manuscript received January 21, 2018; revised April 26, 2018; accepted May 25, 2018. Date of publication June 5, 2018; date of current version December 7, 2018. This work was supported in part by the National Natural Science Foundation of China under Grant 51522704 and Grant 51477154 and in part by the Zhejiang Natural Science Outstanding Young Scholar Foundation (LR18070001). Recommended for publication by Associate Editor H. Peng. *(Corresponding author: Xinke Wu.)*

The authors are with the College of Electrical Engineering, Zhejiang University, Hangzhou 310027, China (e-mail:

TABLE I
SUMMARY OF DUT

Parameters	Device A	Device B	Device C
Voltage/Current Rating	600V/35A	650V/30A	600V/13A
Technology	CoolMOS™	E-mode (p-gate)	E-mode (X-GaN GIT)
Package	TO-220	GaN*PX*®	DFN 8×8
R_{DSON}[a]	53(52/60) mΩ	46(50/63) mΩ	150(140/190) mΩ

[a]. The R_{DSON} values are extracted from the output curves measured by curve tracer at room temperature and the R_{DSON} typical/maximum values from datasheet at 25 °C are also given in parenthesis for reference.

is favorable to simulate a steady-state operating converter in practical applications, has not been discussed in [12]. The drain-to-source voltage applied to DUT during the OFF state is not a square wave under soft-switching condition in [13], which is different from most of the applications. In [16], the dynamic R_{DSON} characteristics under the two switching conditions are evaluated by independently controlling the gate and drain pulses, where the measurement method and circuit are not yet clearly illustrated.

Because GaN device's turn-ON switching loss is much higher than turn-OFF loss [17], the zero-voltage turn-ON circuit is preferred for a GaN-based converter at high-frequency applications. Therefore, from the application perspective, current DPTs or other hard-switching test circuits are not sufficient for a comprehensive investigation of dynamic R_{DSON}. However, few test circuits operating in soft-switching mode have been built for dynamic R_{DSON} evaluation in previous works. A zero-voltage transition (ZVT) circuit was employed in [12] for GaN devices evaluation in soft-switching conditions. Although the ZVT branch can be easily connected or disconnected to the conventional DPT, the additional resonant inductor and the auxiliary switch complicate the test circuit. A resonance-based soft-switching circuit is proposed in [14]. Although there is no voltage or current spikes in the measured waveforms, a long delay time of R_{DSON} measurement still exists and the duty ratio is limited in order to realize zero-voltage-switching (ZVS) conditions.

In this paper, a simple and effective method is proposed for comprehensive investigation of dynamic R_{DSON} including hard- and soft-switching conditions. Compared to the aforementioned soft-switching test circuits, the proposed circuit is based on a widely used soft-switching technique [18]. It has fewer components and can be easily implemented from conventional DPT. The developed circuit and method are used to investigate the dynamic R_{DSON} of the two types of the state-of-the-art commercial GaN devices in comparison with a Si MOSFET. The key parameters of DUT are listed in Table I. The proposed test method and initial experimental results are reported in [19]. More details about the measurements and mechanism analysis are presented in this paper.

II. Test Setup and Design Considerations

Two test circuits are built for R_{DSON} evaluation of GaN devices. One is the widely used DPT with half-bridge configuration for hard-switching condition. The other is the proposed triangular current-mode (TCM) test circuit for soft-switching condition. The two circuits are integrated into one test board to ensure that a GaN device can be tested by different circuits in the same test setup.

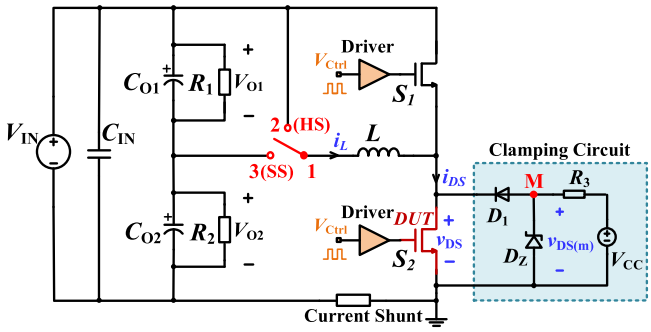

Fig. 1. Test circuit in half-bridge configuration with clamping circuit. The circuit can realize hard-switching (HS) test by connecting 1 to 2 and soft-switching (SS) test by connecting 1 to 3.

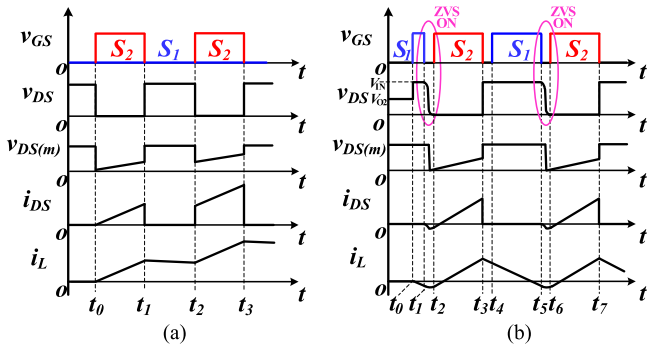

Fig. 2. Control signals and related voltage/current waveforms under (a) hard-switching condition and (b) soft-switching condition.

The test circuit schematic is shown in Fig. 1. A DPT can be built for hard-switching test by connecting 1 to 2. The control signals and related voltage/current waveforms are depicted in Fig. 2(a). The inductor current freewheeling path is provided by the upper device operating in reverse conduction mode. Details about measurement issues of DPT can be found in [20] and [21].

By connecting 1 to 3 in Fig. 1, the test circuit can be converted to a TCM soft-switching circuit. It is similar to a synchronous buck converter, but the output capacitors have already been charged with initial values V_{O1} and V_{O2} before gate signals arrived, due to the series connection of C_{O1} and C_{O2}. Therefore, it can be forced to operate in pulse mode but steady state without initial precharge process for the output capacitors. The control signals and the related voltage/current waveforms are shown in Fig. 2(b). First, during t_0–t_1, a narrow-pulse gate signal (around 100 ns) is given to the upper device S_1. S_1 conducts for a short while with the load inductor charged by $V_{IN}-V_{O2}$ and load current i_L increasing to a small value. During the deadtime t_1–t_2, i_L discharges the parasitic capacitance of S_2, so the v_{DS} of S_2 begins to drop. When v_{DS} drops to zero, the channel of S_2 then begins to conduct reversely. Subsequently, S_2 can be turned ON under ZVS at t_2. As S_2 is turned ON, the load inductor is

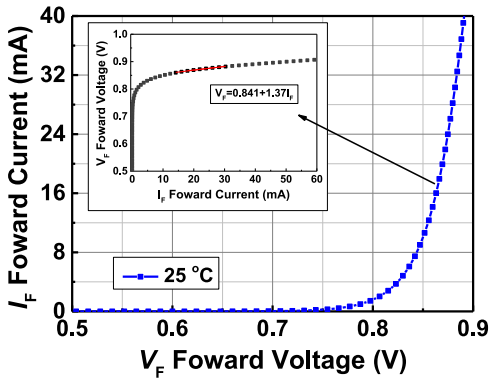

Fig. 3. *I–V* characteristics of D_1 at 25 °C. Inset: Fitting formula between I_F and V_F.

reversely charged by $V_{IN}-V_{O1}$. The load current i_L changes the direction and keeps increasing until S_2 is turned OFF at t_3. After a deadtime, S_1 is turned ON again at t_4 with decreasing i_L and finally turned OFF at t_5, which lead to the next ZVS turn ON of S_2 at t_6. The deadtime used in this design is 100 ns which is within a reasonable range to realize ZVS. The capacity of C_{O1} and C_{O2} is large enough to keep V_{O1} and V_{O2} constant during the microsecond-level test. The values of V_{O1} and V_{O2} can be determined by resistors R_1 and R_2, which enable the converter to go directly into steady state at different duty cycles in multipulse test mode. Here, R_1 and R_2 are the same to match 50% duty cycle.

Based on the test circuits, the R_{DSON} can be obtained by measuring ON-state voltage and drain current. In order to measure the low ON-state voltage after switching from high-voltage OFF state, a fast and accurate clamping circuit is required. Several circuits for high-accuracy measurement of ON-state voltage are proposed in previous literatures. Considering the effectiveness and simplicity of implementation, the clamping circuit in [22] is selected and simplified for R_{DSON} evaluation in this paper. As shown in Fig. 1, The voltage drop $v_{DS(m)}$ across the Zener diode D_Z is measured instead of the real drain to source voltage v_{DS} of DUT. During the OFF state of DUT, the diode D_1 is OFF, so $v_{DS(m)}$ is clamped to the Zener voltage of D_Z, which is much lower than v_{DS}. When DUT is turned ON, the junction capacitance of D_1 is discharged until D_1 is turned ON. As a result, $v_{DS(m)}$ represents the sum of v_{DS} and the diode forward voltage v_{D1}. Different from that in [22], v_{D1} here is calibrated rather than using a constant value in that the variation of v_{D1} will affect measurement accuracy especially for low R_{DSON} devices. The *I–V* characteristics of D_1 shown in Fig. 3 are measured by Agilent HP4155B semiconductor parameter analyzer. A fitting formula is obtained between the forward voltage V_F and the forward current I_F to calibrate v_{D1}. To avoid junction temperature rising of D_1, the value of R_3 is selected carefully to keep the forward current low.

It is noteworthy that the first valid R_{DSON} data should be taken after about 150 ns delay from turn ON because of the ringing caused by junction capacitance discharge of D_1 during the switching transient, although a SiC Schottky diode (CSD01060) with small parasitic capacitance is used here.

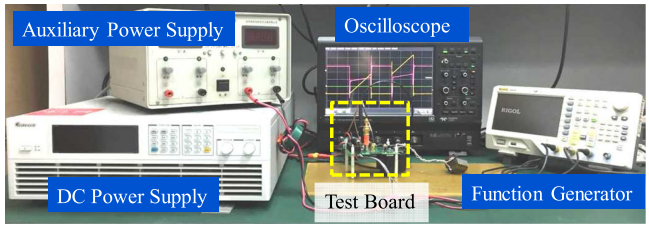

Fig. 4. Test setup for dynamic R_{DSON} evaluation.

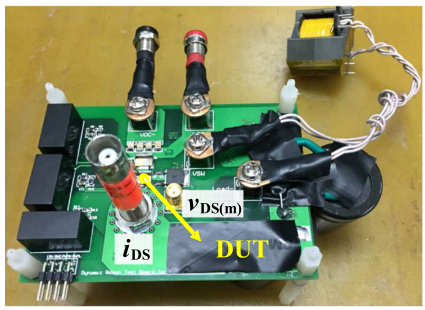

Fig. 5. Photo of the four-layer PCB test board.

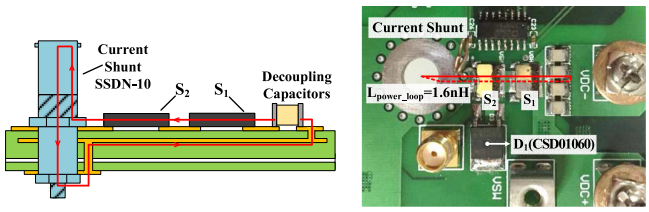

Fig. 6. (a) Low-inductance power loop design for the half-bridge configuration. (b) Top view of the test board.

The test system setup and the test board are depicted in Figs. 4 and 5, respectively. The printed circuit board (PCB) layout is optimized with low parasitic inductance. As shown in Fig. 6(a), both the upper and lower devices are located on the top of the PCB with a group of decoupling capacitors closely sits on the same side. The current return path is placed in the midlayer to make the loop current flow in parallel and opposite directions, aiming at magnetic flux cancellation and parasitic inductance reduction. The power loop inductance introduced by PCB layout is only 1.6 nH as extracted from Ansys Q3D simulation at 1 MHz [see Fig. 6(b)]. Three test boards with the same configuration have been built to accommodate different packages of the three types of devices. In more detail, an isolated half-bridge driver IC ADUM3223 is used with 10-Ω turn-ON gate resistor and 5-Ω turn-OFF gate resistor, respectively.

The drain current is measured with a 0.1-Ω coaxial shunt (SSDN-10) from T&M Research, Inc. An SMA connector with coaxial cable is used to sense the clamping voltage. For more accurate measurement of R_{DSON}, it is necessary to ensure that the propagation delay between voltage and current probes are calibrated before measurement. The alignment of voltage and current measurement is achieved by replacing the DUT with a low-inductance resistor and measuring the voltage and current of the resistor at the same time [21].

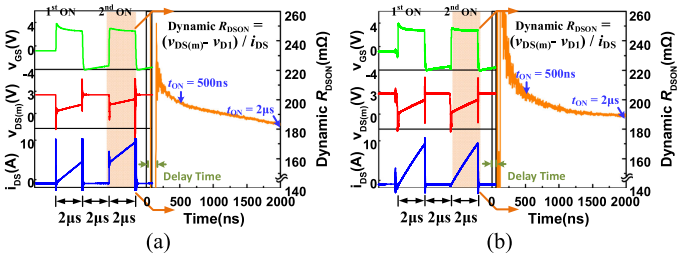

Fig. 7. Measurement and extraction method for the valid data points of dynamic R_{DSON} in double-pulse operating mode. The time slot for the R_{DSON} measuring is shown in the shadow region. (a) Hard-switching condition. (b) Soft-switching condition.

III. Double-Pulse Test Under Hard- and Soft-Switching Conditions

A. Dynamic R_{DSON} Measurement Method

Fig. 7 illustrates the measurement and extraction method for the valid data points of dynamic R_{DSON} in double-pulse operating mode. The DUT conducts 2 μs during the first pulse. After a short interval of 2 μs, the DUT is turned ON again due to the second 2-μs pulse. Dynamic R_{DSON} variations are measured and calculated during the second on-state time highlighted in Fig. 7. Since R_{DSON} is not a constant value during the on-state time and decreases gradually after switching from high-voltage OFF state, the dynamic R_{DSON} at 500 ns (the beginning of conduction) and 2 μs (the end of conduction) are extracted to describe this process. The selection of 500 ns aims at avoiding switching noise at the beginning of conduction. For each DUT, the R_{DSON} is measured under different voltage stresses from 50 to 400 V (50 V per step) with the same drain current. The same drain current under different voltage stresses can be maintained by adjusting the value of the external inductor proportionally.

B. Experimental Results

Fig. 8 shows the measured R_{DSON} variation of the three DUTs (devices A, B, and C) under hard- and soft-switching conditions, respectively. The time point when v_{GS} begin to rise is set as the origin of the time axis. The missing R_{DSON} data during the initial part of time axis suggest the measurement delay time, which is observed within 150 ns. It should be mentioned that under soft-switching condition, the large oscillations during the first 500 ns are caused by the low i_{DS} at the beginning of conduction.

The measured R_{DSON} values are normalized by the static R_{DSON} extracted from output curves measured by curve tracer at the room temperature. The dynamic/static R_{DSON} values at 500 and 2000 ns after turn on from different voltage stresses under hard- and soft-switching conditions are plotted in Fig. 9.

It is obvious that three devices have different R_{DSON} variation trends with varied voltage stress. As expected, there is no dynamic R_{DSON} effect in device A because it is a Si CoolMOS [see Fig. 9(a)]. For device B shown in Fig. 9(b), the dynamic R_{DSON} under hard- and soft-switching conditions exhibit similar variation trends with increasing voltage stress but a little bit lower R_{DSON} is observed under soft-switching condition.

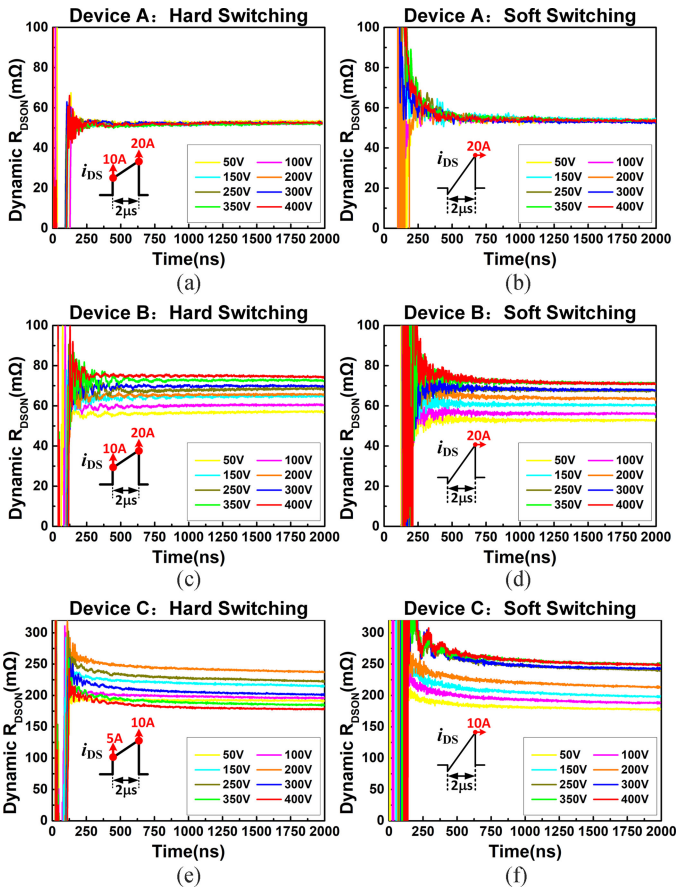

Fig. 8. Dynamic R_{DSON} under hard- and soft-switching conditions with different voltage stresses from 50 to 400 V with the same drain current. (a) and (b) Device A. (c) and (d) Device B. (e) and (f) Device C. Inset: Drain current variation during the measurement period.

The results are consistent with a general understanding of GaN devices from previous works [10], [12], [13].

However, device C shows different characteristics. First, as shown in Fig. 9(c), the R_{DSON} exhibits nonmonotonic behavior under hard switching with increasing voltage stress. The maximum R_{DSON} can be deduced at the turning voltage stress which is between 200 and 250 V. It is observed that the dynamic R_{DSON} in the DUT is nearly the same to the static R_{DSON} under high-voltage stress (400 V). Second, an obvious increase of dynamic R_{DSON} under soft-switching condition is observed, which is more severe under high-voltage switching condition (400 V). Similar phenomenon has been shown in [16], where the GaN HFETs under test showed higher R_{DSON} under soft-switching condition, but the physical mechanism is different due to the different device structures between device C here and the DUT in [16]. Third, soft-switching condition results in lower R_{DSON} below the turning voltage stress but higher R_{DSON} above the turning voltage stress, as compared to the hard-switching condition.

The different experimental results of devices B and C originate from different device structures and technologies. The major difference between the two types of devices is that the device C is fabricated with an additional p-GaN structure in the vicinity of the drain electrode (PD) [6], while such structure does not

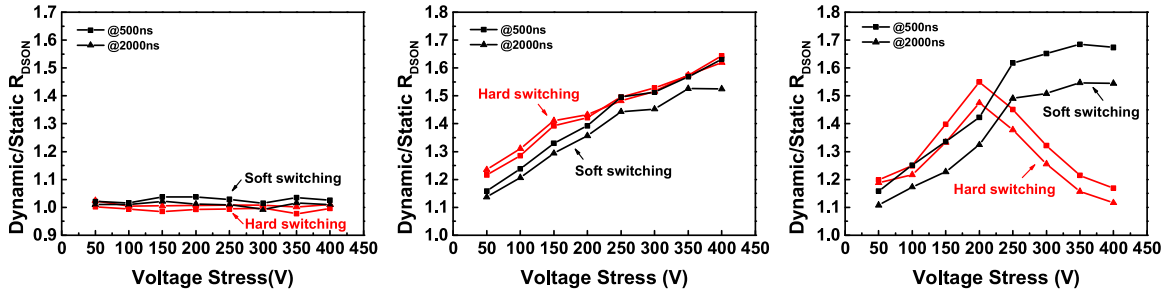

Fig. 9. Dynamic/static R_{DSON} values at 500 and 2000 ns after turn ON from different voltage stresses under hard- and soft-switching conditions. (a) Device A. (b) Device B. (c) Device C.

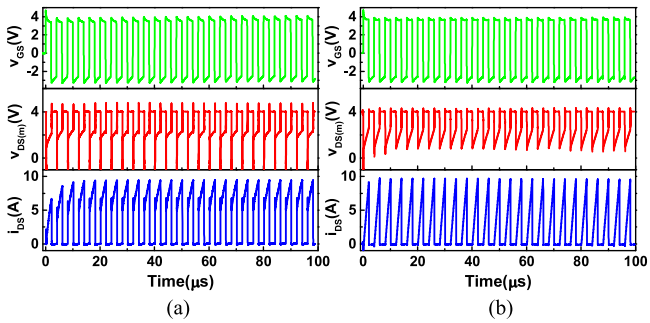

Fig. 10. Multipulse test waveforms at $V_{\mathrm{DS}} = 100\,\mathrm{V}$ and $f = 250\,\mathrm{kHz}$. (a) Under hard-switching condition. (b) Under soft-switching condition.

exist in device B. The impact of PD on the dynamic R_{DSON} and its underlying mechanism will be discussed in Section V.

The experimental results reveal the impact of switching conditions on dynamic R_{DSON} due to different device structures and technologies. Therefore, for current commercial GaN power devices, it is inappropriate to evaluate current collapse characteristics without considering switching conditions, which may lead to an inaccurate evaluation of dynamic R_{DSON} and errors in loss estimation.

IV. Multipulse Test Under Hard- and Soft-Switching Conditions

The trapping and detrapping effect of GaN device is similar to the charging and discharging process of *RC* units in series with specific time constants [23], [24]. It suggests that the dynamic R_{DSON} requires sufficient time to reach the steady state and the settling time could depend on the switching frequency. Therefore, a multipulse test mode with different frequencies needs to be taken into considerations.

A. Dynamic R_{DSON} Measurement Method

In this test mode, only devices B and C are tested. Fig. 10 shows the key waveforms of dynamic R_{DSON} evaluation in multipulse test mode. The total test time is limited to 100 μs to avoid self-heating. For a hard-switching test, the inductance load in Fig. 1(a) is replaced by an *RL* load (resistor and inductor in series) to set up inductor volt–second balance, and, consequently, avoid the continuous increase of a drain current. For a soft-switching test, the test circuit is the same to that of the double-pulse test mode.

For each DUT, the dynamic R_{DSON} is measured at 250 kHz, 500 kHz, and 1 MHz under different voltage stresses from 100 to 400 V (100 V per step) with the same drain current. For hard switching, the values of the *RL* load are adjusted carefully to ensure the same drain current under different conditions and the drain current can reach the steady state within 10 μs. For soft switching, the drain current increases from zero to the steady-state value during each cycle. Meanwhile, the impact of frequency on the dynamic R_{DSON} at different voltage stresses is observed. The duty cycles in all cases are set as 50%.

B. Experimental Results

Dynamic R_{DSON} during the total 100-μs test period of device B and device C are shown in Figs. 11 and 12, respectively, where Figs. 11(e)–(h) and 12(e)–(h) enlarge the final conduction period in detail. For clarity, only 100- and 400-V conditions are shown here. In order to reflect the R_{DSON} in quasi-steady state, the median value of R_{DSON} during the final conduction period is extracted for comparison.

Fig. 13 summarizes the normalized R_{DSON} value with various voltage stresses. Similar to the double-pulse test results, R_{DSON} of device B increases with voltage stress under both hard- and soft-switching conditions while lower R_{DSON} can be observed under soft switching. R_{DSON} of device C exhibits nonmonotonic behavior under hard switching with increasing voltage stress where there is still a turning voltage between 200 V and 300 V. It has been found that the soft switching results in lower R_{DSON} below the turning voltage but higher R_{DSON} above the turning voltage, as compared to the hard switching condition.

The measured R_{DSON} are replotted in Fig. 14 with the various frequencies. It is well acknowledged that higher frequency results in an increase of dynamic R_{DSON} and the increase is more apparent with higher voltage stress due to more severe trapping effect [11], which coincides with the experimental results. In addition, the experimental results also show that the impact of frequency on R_{DSON} depends on switching conditions and device structure. As shown in Fig. 14, for device B without PD structure, the measured R_{DSON} is relatively insensitive to the switching frequency, especially in soft-switching condition. For device C with PD structure, the dynamic R_{DSON} increases with frequency under both hard- and soft-switching conditions. The

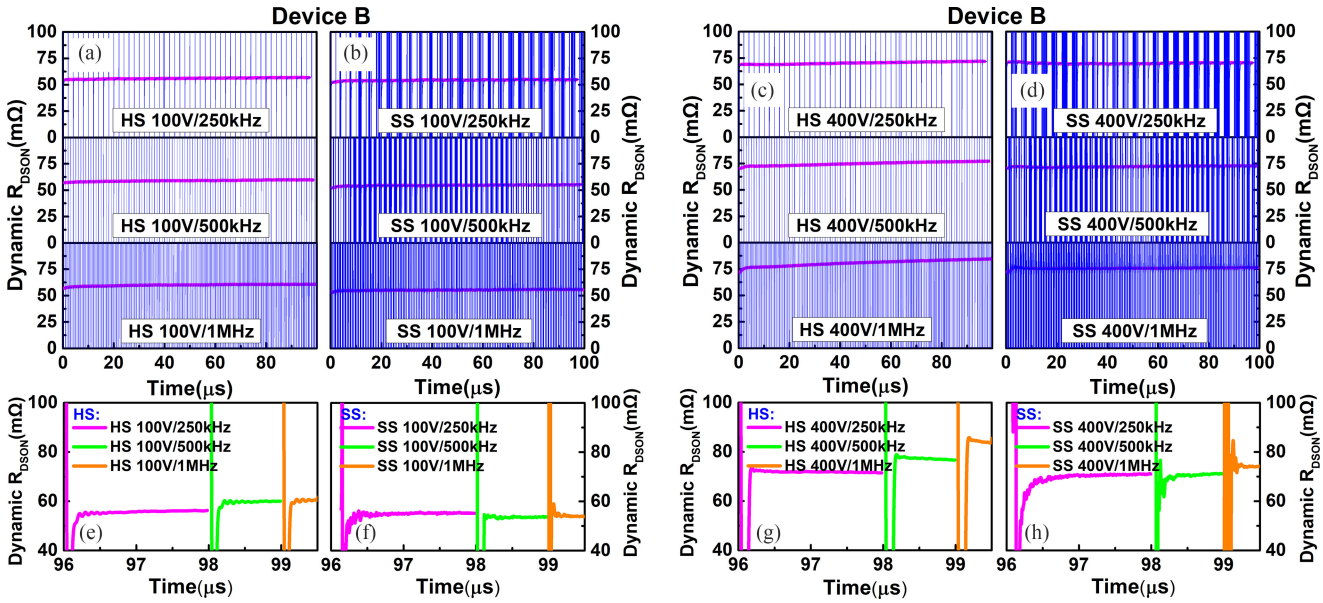

Fig. 11. Dynamic R_{DSON} variation of device B during the total 100-μs test period under hard-switching (HS) and soft-switching (SS) conditions with different frequencies. (a), (b) At 100-V voltage stress. (c), (d) At 400-V voltage stress. (e), (f) R_{DSON} variation during the final pulse at 100-V voltage stress with different frequencies. (g), (h) R_{DSON} variation during the final pulse at 400-V voltage stress with different frequencies.

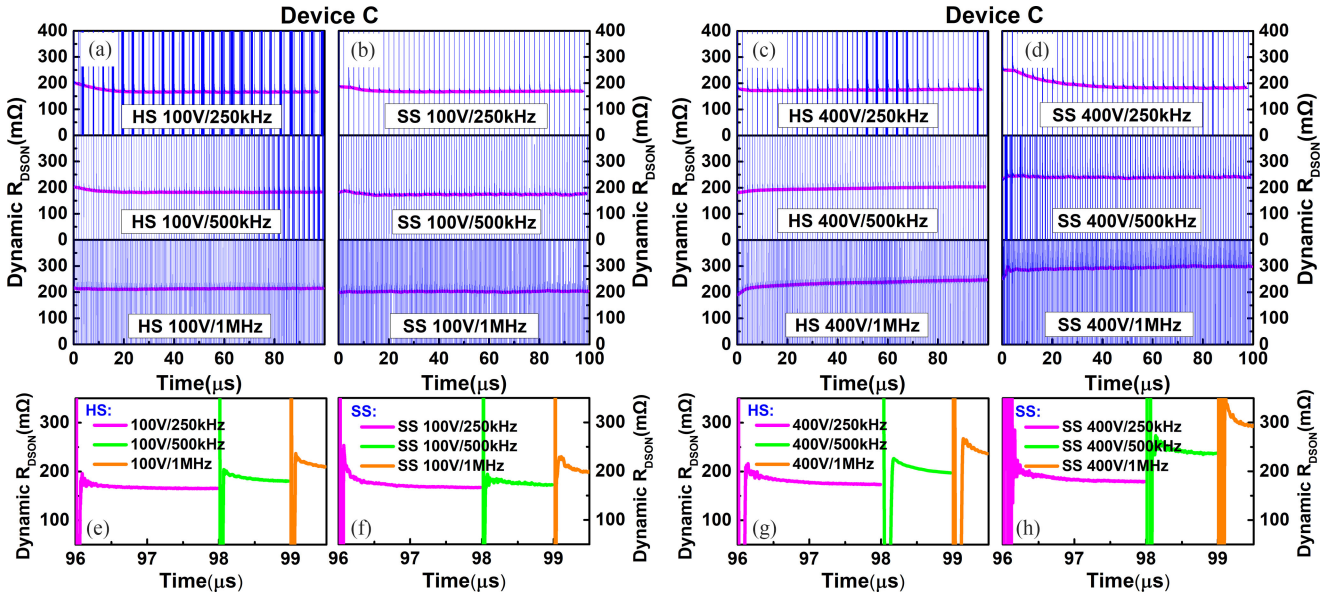

Fig. 12. Dynamic R_{DSON} variation of device C during the total 100-μs test period under hard-switching (HS) and soft-switching (SS) conditions with different frequencies. (a), (b) At 100-V voltage stress. (c), (d) At 400-V voltage stress. (e), (f) R_{DSON} variation during the final pulse at 100-V voltage stress with different frequencies. (g), (h) R_{DSON} variation during the final pulse at 400-V voltage stress with different frequencies.

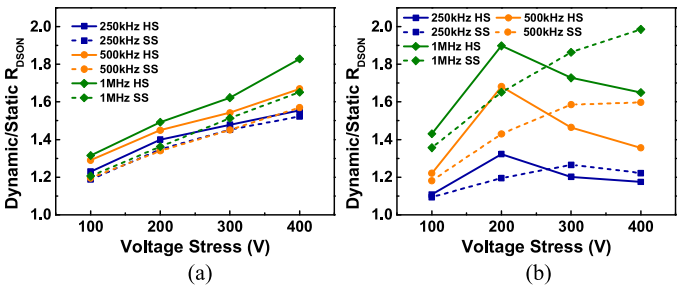

Fig. 13. Dynamic/static R_{DSON} with different voltage stresses under hard- and soft-switching conditions. (a) Device B. (b) Device C.

difference in R_{DSON} under the two switching conditions is more obvious at high voltage and high frequency. Especially when operating under 400-V and 1-MHz soft-switching condition, the dynamic R_{DSON} becomes nearly twice as the static value, which indicates a very serious current collapse.

It is noteworthy from Fig. 12(a)–(d) that the dynamic R_{DSON} varies gradually to a nearly steady value with the increase of pulse number. The pulse numbers needed to reach the steady state are different with frequency and voltage stress. For clarity, the median value of R_{DSON} during each conduction period at 250 kHz is extracted and plotted in Fig. 15, where the results

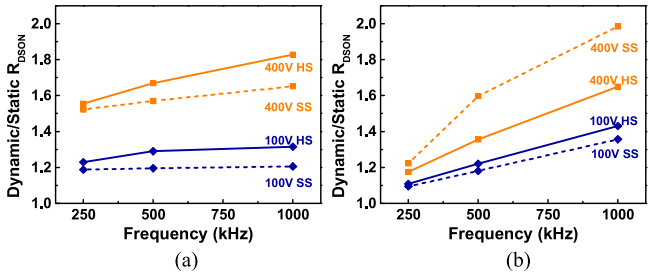

Fig. 14. Dynamic/static R_{DSON} with different frequencies at 100 and 400 V under hard- and soft-switching conditions. (a) Device B. (b) Device C.

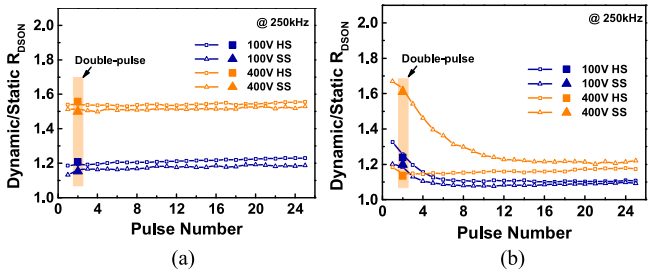

Fig. 15. Dynamic/static R_{DSON} variation with pulse number at $f = 250$ kHz multipulse operating mode (symbol line). The results of double-pulse test mode are denoted by larger symbols. (a) Device B. (b) Device C.

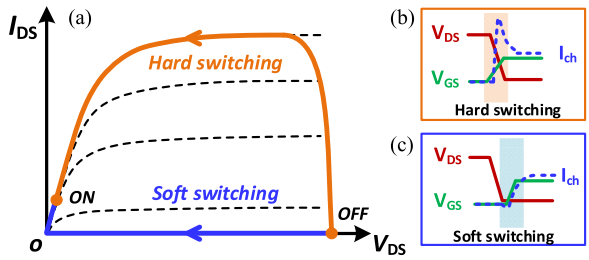

Fig. 16. (a) Load line during the switching transient. (b) Hard-switching transient cause high channel current. (c) Soft-switching transient cause low channel current.

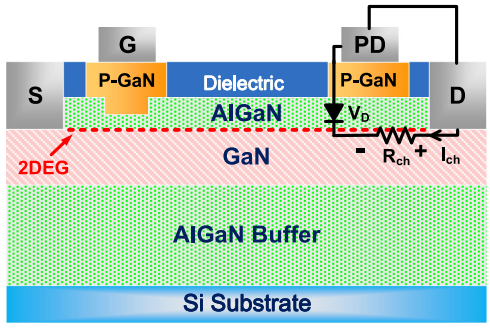

Fig. 17. Schematic cross section of GaN device with an additional p-GaN drain (PD). The PD structure and the 2DEG channel form a p-n junction.

of double-pulse test mode are also denoted. It is obvious that for device B, the double-pulse results are consistent well with that of multipulse, while for device C, the double-pulse results cannot reflect the true R_{DSON} in a steady state due to the time-dependent trapping and detrapping effect. It suggests that the traditional test method using only one or two pulses may not be sufficient with respect to the dynamic R_{DSON} evaluation of current commercial GaN devices due to their different device technologies.

V. Mechanism Analysis

Previous publications have paid much attention to the impact of different operation parameters on dynamic R_{DSON} including OFF-state time, voltage, temperature, etc., but few of them provide specific explanation of the experimental results. This section aims to further enhance the understanding of the dynamic R_{DSON} under different switching conditions and the analysis results can provide valuable information for both applications and device manufacturing.

Fig. 9(b) shows that dynamic R_{DSON} of device B under hard- and soft-switching conditions exhibit similar variation trends with OFF-state voltage, but a lower R_{DSON} is observed under soft-switching condition. The results are consistent with a general understanding of GaN devices in previous works [10], [12], [13], which is attributed to enhanced hot electron effect during hard switching [2].

Fig. 16(a) illustrates the load lines under different switching conditions. For hard switching, the load line passes through high-power area with high voltage and high current applied simultaneously, resulting in hot electron injection to surface traps as well as buffer traps and R_{DSON} increase [2]. For soft switching, the effect of hot electron is not prominent since the load line bypass the high-power area. Consequently, the R_{DSON} is lower under soft-switching condition. The hot electron effect becomes more obvious at high-voltage stress and high frequency under hard-switching condition, which is responsible for R_{DSON} increase with OFF-state voltage and frequency [2], [25]. The measured R_{DSON} is relatively insensitive to the switching frequency in soft-switching condition [see Fig. 14(a)] due to minimal hot electron effect which usually occurs under hard-switching condition.

For device C, the nonmonotonic R_{DSON} behavior with increasing voltage stress under hard-switching condition shown in Fig. 9(c) suggests an additional mechanism. Compared with device B, the PD structure in device C (shown in Fig. 17) is beneficial to alleviate current collapse since the injected holes from PD during the hard-switching transient can effectively release the trapped electrons near the drain [6]. However, the performance of PD is affected by switching conditions and voltage stress from the experimental results.

To explain the physical mechanisms of the experimental results and further investigate the impact of switching conditions on R_{DSON}, a normally OFF AlGaN/GaN GIT with PD is modeled, using the device structure presented in [26] for reference. The schematic cross section of the device is shown in Fig. 17.

As shown in Fig. 17, the PD structure and the 2DEG channel form a p-n junction with a built-in voltage V_{F}, where PD serves as the anode and 2DEG channel serves as the cathode [27]. The voltage drop V_{D} across the p-n junction is determined by

$$V_D = I_{\mathrm{ch}} \times R_{\mathrm{ch}} \tag{1}$$

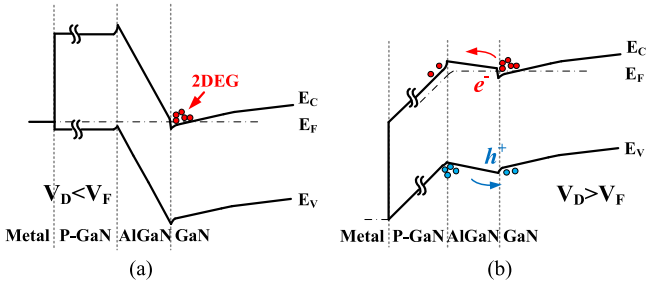

Fig. 18. Schematic energy band diagrams of the p-n junction. (a) $V_D < V_F$. (b)$V_D > V_F$.

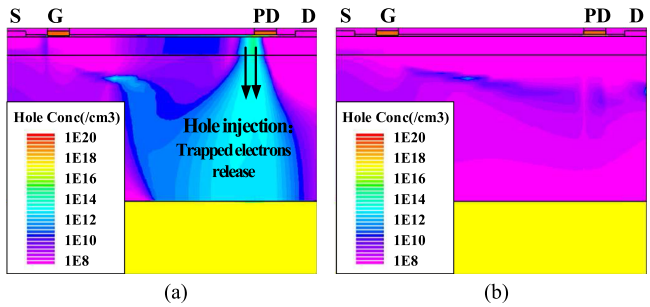

Fig. 19. Device schematic cross section at turn-ON transient after 2-μs 400-V stress. (a) Hard-switching condition: Hole injection from PD due to high channel current. (b) Soft-switching condition: Insignificant hole injection effect due to low channel current at the switching transient.

where I_{ch} is the channel current and R_{ch} is the channel resistance between the cathode and the drain electrode. The schematic energy band diagrams of the p-n junction are shown in Fig. 18. When $V_D > V_F$, holes can be injected from the p-GaN region to the buffer layer.

During hard-switching turn-ON transient at high drain voltage, as shown in Fig. 16(b), high channel current I_{ch} causes voltage drop V_D across the p-n junction (exceeds V_F), resulting in the hole injection into buffer stack from PD, which can effectively release the trapped electrons near the drain, and, therefore, suppress current collapse. However, when operating under soft turn-ON condition, the voltage stress at PD drops to near zero before the channel turns ON, resulting in very low current through the channel at the transient, as shown in Fig. 16(c). Therefore, the p-n junction cannot be switched ON due to $V_D < V_F$. Thus, the hole injection effect cannot be activated which leads to higher dynamic R_{DSON}.

The trapping mechanisms and impact of hole injection under different switching conditions are analyzed by Silvaco TCAD tool. The device is switched ON after 2-μs voltage stress of 400 V under both hard- and soft-switching conditions. Different switching conditions are realized by adjusting the overlap between the given V_{GS} and V_{DS} waveforms. Simulation result in Fig. 19(a) verifies the hole injection phenomenon from PD structure at hard-switching transient, while Fig. 19(b) shows insignificant hole injection effect at soft-switching transient. The simulation result in Fig. 20 is in qualitative agreement with the experimental results, i.e., the device with PD structure performs better R_{DSON} characteristics under hard-switching than soft-switching condition at high-voltage stress.

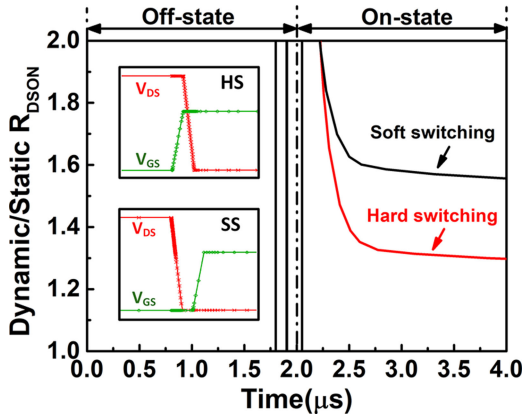

Fig. 20. Simulation results of dynamic/static R_{DSON}. Inset: V_{GS} and V_{DS} waveforms for hard and soft switching.

In summary, there are two distinct mechanisms that cause the nonmonotonic R_{DSON} behavior of device C with increasing voltage stress under hard-switching condition. When operating below the turning voltage stress, the dominant hot electron effect results in increasing R_{DSON} with voltage stress and higher R_{DSON} under hard-switching condition, as compared to soft-switching condition. When operating above the turning voltage stress, the hole injection effect from PD becomes more significant as the voltage stress increase, which results in decreasing R_{DSON} with voltage stress and lower R_{DSON} than soft-switching condition.

VI. Conclusion

In this paper, dynamic R_{DSON} behaviors of two types of state-of-the-art commercial GaN devices are measured and compared under hard- and soft-switching conditions including double-pulse and multipulse operating modes, using the test circuit and technique developed in this study.

It has been found that their dynamic R_{DSON} exhibit different behaviors under hard- and soft-switching conditions due to different device technologies. The experimental results and mechanism discussion reveal the impact of switching conditions on dynamic R_{DSON} and provide valuable insights into the device level for further understanding.

Based on the experiment and simulation analysis, special considerations should be taken for current commercial GaN power devices in terms of dynamic R_{DSON} evaluation.

1) Impact of switching conditions should be taken into consideration. In state-of-the-art GaN power devices, one way to alleviate R_{DSON} degradation is based on hole injection. However, the effectiveness of hole injection strongly depends on switching conditions, which results in different dynamic R_{DSON} behaviors under hard- and soft-switching conditions. Therefore, besides the OFF-state voltage and frequency, switching condition is also a key factor for dynamic R_{DSON} evaluation, especially for the devices using hole injection related technology to suppress current collapse.

2) Multipulse test is preferred to match practical applications. For some GaN devices, the method using single pulse or double pulses could not reflect the R_{DSON} behaviors in a steady-state operating converter since the R_{DSON} varies gradually during each switching cycle before settling down. The variation depends on the trapping and detrapping time constants in each switching period. In this case, the multipulse test method, which operates in a quasi-steady state, is preferred to match the practical applications.

REFERENCES

[1] R. Vetury, N. Q. Zhang, S. Keller, and U. K. Mishra, "The impact of surface states on the DC and RF characteristics of AlGaN/GaN HFETs," *IEEE Trans. Electron Devices*, vol. 48, no. 3, pp. 560–566, Mar. 2001.

[2] I. Hwang *et al.*, "Impact of channel hot electrons on current collapse in AlGaN/GaN HEMTs," *IEEE Electron Device Lett.*, vol. 34, no. 12, pp. 1494–1496, Dec. 2013.

[3] E. A. Jones, F. F. Wang, and D. Costinett, "Review of commercial GaN power devices and GaN-based converter design challenges," *IEEE J. Emerg. Sel. Topics Power Electron.*, vol. 4, no. 3, pp. 707–719, Sep. 2016.

[4] O. Hilt, E. Bahat-Treidel, E. Cho, S. Singwald, and J. Würfl, "Impact of buffer composition on the dynamic on-state resistance of high-voltage AlGaN/GaN HFETs," in *Proc. Int. Symp. Power Semicond. Devices IC's*, 2012, pp. 345–348.

[5] GN001 Application Guide. GaN Systems Inc., Ottawa, ON, Canada. (2018). [Online]. Available: https://gansystems.com

[6] S. Kaneko *et al.*, "Current-collapse-free operations up to 850 V by GaN-GIT utilizing hole injection from drain," in *Proc. Int. Symp. Power Semicond. Devices IC's*, 2015, pp. 41–44.

[7] D. Jin and J. A. del Alamo, "Methodology for the study of dynamic on-resistance in high-voltage GaN field-effect transistors," *IEEE Trans. Electron Devices*, vol. 60, no. 10, pp. 3190–3196, Oct. 2013.

[8] M. Wang *et al.*, "Investigation of surface- and buffer-induced current collapse in GaN high-electron mobility transistors using a soft switched pulsed *I-V* measurement," *IEEE Electron Device Lett.*, vol. 35, no. 11, pp. 1094–1096, Nov. 2014.

[9] N. Badawi, O. Hilt, E. Bahat-Treidel, J. Böcker, J. Würfl, and S. Dieckerhoff, "Investigation of the dynamic on-state resistance of 600 V normally-off and normally-on GaN HEMTs," *IEEE Trans. Ind. Appl.*, vol. 52, no. 6, pp. 4955–4964, Nov./Dec. 2016.

[10] H. Wang, J. Wei, R. Xie, C. Liu, G. Tang, and K. J. Chen, "Maximizing the performance of 650-V p-GaN gate HEMTs: Dynamic R_{ON} characterization and circuit design considerations," *IEEE Trans. Power Electron.*, vol. 32, no. 7, pp. 5539–5549, Jul. 2017.

[11] Y. Cai, A. J. Forsyth, and R. Todd, "Impact of GaN HEMT dynamic on-state resistance on converter performance," in *Proc. Appl. Power Electron. Conf. Expo.*, 2017, pp. 1689–1694.

[12] T. Yao and R. Ayyanar, "A multifunctional double pulse tester for cascode GaN devices," *IEEE Trans. Ind. Electron.*, vol. 64, no. 11, pp. 9023–9031, Nov. 2017.

[13] B. Lu, T. Palacios, D. Risbud, S. Bahl, and D. I. Anderson, "Extraction of dynamic on-resistance in GaN transistors: Under soft- and hard-switching conditions," in *Proc. Compound Semicond. Integr. Circuit Symp.*, 2011, pp. 1–4.

[14] G. Cao, A. Ansari, and H. J. Kim, "A new measurement circuit to evaluate current collapse effect of GaN HEMTs under practical conditions," *IEEE Trans. Instrum. Meas.*, vol. 64, no. 7, pp. 1977–1986, Jul. 2015.

[15] T. Cappello, A. Santarelli, and C. Florian, "Dynamic RON characterization technique for the evaluation of thermal and off-state voltage stress of GaN switches," *IEEE Trans. Power Electron.*, vol. 33, no. 4, pp. 3386–3398, Apr. 2018.

[16] J. Joh, N. Tipirneni, S. Pendharkar, and S. Krishnan, "Current collapse in GaN heterojunction field effect transistors for high-voltage switching applications," in *Proc. Int. Rel. Phys. Symp.*, 2014, pp. 6C.5.1–6C.5.4.

[17] X. Huang, T. Liu, B. Li, F. C. Lee, and Q. Li, "Evaluation and applications of 600V/650V enhancement-mode GaN devices," in *Proc. Workshop Wide Bandgap Power Devices Appl.*, 2015, pp. 113–118.

[18] X. Huang, Z. Liu, F. C. Lee, and Q. Li, "Characterization and enhancement of high-voltage cascode GaN devices," *IEEE Trans. Electron Devices*, vol. 62, no. 2, pp. 270–277, Feb. 2015.

[19] R. Li, X. Wu, G. Xie, and K. Sheng, "Dynamic on-state resistance evaluation of GaN devices under hard and soft switching conditions," in *Proc. IEEE Appl. Power Electron. Conf. Expo.*, 2018, pp. 898–903.

[20] J. B. Witcher, "Methodology for switching characterization of power devices and modules," M.S. thesis, Dept. Electr. Eng., Virginia Polytech. Inst. State Univ., Blacksburg, VA, USA, 2002.

[21] Z. Zhang, B. Guo, F. F. Wang, E. A. Jones, L. M. Tolbert, and B. J. Blalock, "Methodology for wide band-gap device dynamic characterization," *IEEE Trans. Power Electron.*, vol. 32, no. 12, pp. 9307–9318, Dec. 2017.

[22] N. Badawi and S. Dieckerhoff, "A new method for dynamic R_{on} extraction of GaN power HEMTs," in *Proc. Int. Exhib. Conf. IEEE Power Electron. Intell. Motion, Renew. Energy Energy Manage.*, 2015, pp. 1–6.

[23] J. Böcker, H. Just, O. Hilt, N. Badawi, J. Würfl, and S. Dieckerhoff, "Experimental analysis and modeling of GaN normally-off HFETs with trapping effects," in *Proc. Eur. Conf. Power Electron. Appl.*, 2015, pp. 1–10.

[24] K. Li, P. L. Evans, and C. M. Johnson, "Characterisation and modeling of gallium nitride power semiconductor devices dynamic on-state resistance," *IEEE Trans. Power Electron.*, vol. 33, no. 6, pp. 5262–5273, Jun. 2018.

[25] M. Meneghini, A. Stocco, R. Silvestri, N. Ronchi, G. Meneghesso, and E. Zanoni, "Impact of hot electrons on the reliability of AlGaN/GaN high electron mobility transistors," in *Proc. Int. Rel. Phys. Symp.*, 2012, pp. 2C.2.1–2C.2.5.

[26] K. Tanaka *et al.*, "Suppression of current collapse by hole injection from drain in a normally-off GaN-based hybrid-drain-embedded gate injection transistor," *Appl. Phys. Lett.*, vol. 107, no. 16, Oct. 2015, Art. no. 163502.

[27] X. Tang, B. Li, Z. Zhang, G. Tang, J. Wei, and K. J. Chen, "Characterization of static and dynamic behaviors in AlGaN/GaN-on-Si power transistors with photonic-ohmic drain," *IEEE Trans. Electron Devices*, vol. 63, no. 7, pp. 2831–2837, Jul. 2016.

Rui Li (S'18) received the B.S. degree in electrical engineering from Zhejiang University, Hangzhou, China, in 2016, where she is currently working toward the M.S. degree at the College of Electrical Engineering.

Her current research interests include wide-bandgap power semiconductor devices and gate drive techniques.

Xinke Wu (M'09) received the B.S. degree and M.S. degree in electrical engineering from the Harbin Institute of Technology, Harbin, China, in 2000 and 2002, respectively, and the Ph.D. degree in electrical engineering from Zhejiang University, Hangzhou, China, in 2006.

He was a Postdoctoral Fellow with the National Engineering Research Center for Applied Power Electronics, Zhejiang University, from 2007 to 2009. From 2011 to 2012, he was a Visiting Scholar with the Center of Power Electronics System, Virginia Tech. Since 2009, he has been with the Institute of Power Electronics, Zhejiang University, first as an Assistant Research Fellow from 2009 to 2010, then as an Associate Professor from 2011 to 2015, and currently as a Professor. His research interests include high frequency, high power density, and high-efficiency power conversion, power electronics system integration, and high-efficiency LED driving technology.

Dr. Wu received the Young Scholar Award from Zhejiang University in 2012, the Young Scholar Award from NSF of China in 2015, and the Young Scholar Award from CPSS of China in 2017.

Shu Yang (S'12–M'14) received the B.S. degree from Fudan University, Shanghai, China, in 2010, and the Ph.D. degree from the Hong Kong University of Science and Technology, Hong Kong, in 2014.

She is currently an Associate Professor with the College of Electrical Engineering, Zhejiang University, Hangzhou, China.

Kuang Sheng (M'99–SM'08) received the B.Sc. degree from Zhejiang University, Hangzhou, China, in 1995, and the Ph.D. degree from Heriot-Watt University, Edinburgh, U.K., in 1999.

He is currently a Professor with Zhejiang University. His current research interests include all aspects of power semiconductor devices and ICs on SiC and Si.